Journal of Applied Physics

Cascaded InGaSb quantum dot mid-infrared LEDs

Cite as: J. Appl. Phys. **131**, 043105 (2022); https://doi.org/10.1063/5.0072984
Submitted: 26 September 2021 • Accepted: 11 January 2022 • Published Online: 28 January 2022

A. J. Muhowski, A. Kamboj, A. F. Briggs, et al.

Journal of Applied Physics ARTICLE scitation.org/journal/jap

Cascaded InGaSb quantum dot mid-infrared LEDs

Cite as: J. Appl. Phys. **131**, 043105 (2022); doi: 10.1063/5.0072984
Submitted: 26 September 2021 · Accepted: 11 January 2022 ·
Published Online: 28 January 2022

A. J. Muhowski, A. Kamboj, A. F. Briggs, L. Nordin, S. R. Bank, and D. Wasserman[a)]

AFFILIATIONS

Department of Electrical and Computer Engineering, University of Texas at Austin, Austin, Texas 78758, USA

[a)]**Author to whom correspondence should be addressed:** dw@utexas.edu

ABSTRACT

We demonstrate cascaded, mid-infrared light-emitting diodes with quantum dot based active regions. Cascading is achieved through highly reverse-biased AlInAsSb tunnel junctions that serve to connect the successive InGaSb quantum dot active regions. Temperature-dependent characterization of the output irradiance as a function of the current and voltage indicates that the cascade architecture has minimal leakage currents in contrast to earlier single-stage devices and provides carrier recycling with a concomitant increase in irradiance. The results show that cascaded architectures can be applied to quantum dot platforms and that the quantum efficiency of the active region limits the overall device efficiency.

I. INTRODUCTION

Mid-infrared (MIR) light-emitting diodes (LEDs) are a sought-after technology poised to replace blackbody light sources for a host of spectroscopic sensing and defense applications where cost, operating power, and/or spectral bandwidth requirements render MIR lasers less than ideal.[1,2] Efforts to develop high-efficiency MIR LEDs have largely focused on mechanisms to mitigate the high non-radiative Auger recombination prevalent in narrow-gap, bulk III–V semiconductor materials. While recent efforts have begun to explore less-mature group IV and IV–VI epitaxial material systems that may exhibit lower bulk Auger coefficients,[3–5] band structure engineering in III–V semiconductors, often employing type-II quantum wells and superlattices with carefully chosen layer thicknesses and compositions, has been the primary method to reduce parasitic Auger recombination.[6–8] Bearing in mind energy and momentum conservation requirements, careful design of the active region band structure allows for the control of the position of electron/hole subband energies in such a way as to minimize Auger recombination, thereby enhancing the efficiency of the MIR active region.

In addition to improving active region quantum efficiency, advanced heterostructures are often employed in tandem with high-efficiency active regions to further increase wallplug efficiency. Cascaded active regions have been a key factor in the development of high-efficiency MIR laser sources, and the III–V class of semiconductors have clusters of lattice-matched alloy families that offer exceptional opportunities to create heterostructure-engineered, cascaded devices. A single carrier transiting across an N stage device is recycled N times, effectively being injected as an excited carrier into each subsequent active region, thus, theoretically allowing a single injected carrier to emit up to N photons. Active region cascading in the MIR was initially demonstrated in the unipolar quantum cascade laser (QCL).[9] However, the intersubband active regions in QCLs have dipole matrix elements polarized entirely in the growth direction and short nonradiative upper state lifetimes that combine to yield exceedingly limited sub-threshold, surface-normal emission. Thus, QCLs are not commonly considered as candidates for applications requiring MIR LEDs. The interband cascade laser (ICL),[10] the interband cousin of the QCL, can provide sub-threshold spontaneous emission and has been leveraged for high-efficiency interband cascade light-emitting devices (ICLEDs).[11] Further, it is worth noting that the majority of ICL and ICLED devices make use of "W" quantum wells, band-structure-engineered to suppress intrinsic Auger processes at the active region level. Other MIR LED systems have employed disparate active regions such as type-I quantum wells[12] and extensively band-structure-engineered type-II superlattices,[13,14] both of which have been utilized in cascaded architectures leveraging reverse-biased *pn* tunnel junctions. While some of the laser-specific advantages of cascading have no effect on spontaneous emitters such as LEDs, cascaded LEDs still benefit from increased wallplug efficiency due to the reduction of Ohmic losses in contacts and transport layers and operate at more conventional voltages.

Epitaxially grown self-assembled quantum dots (QDs), long-considered as potential active regions for a range of optoelectronic devices, have recently seen a resurgence of interest for potential applications in quantum information and silicon integrated photonics.[15,16] Historically, the majority of epitaxial QD research has centered on leveraging the interband transitions in InAs QDs in (Al)GaAs matrices for optoelectronic applications at near-infrared wavelengths. This is, in part, due to the technological maturity of the GaAs-based materials and the potential for integration with commercial telecommunication hardware. Numerous other III–V, III-nitride, and group IV materials[17] have also been explored for a variety of different applications and wavelength ranges. Again, much of this work has typically been at visible or near-IR wavelengths, though efforts have been made to extend QD optoelectronics to the MIR by leveraging intersubband transitions in the QDs,[18,19] most successfully in the case of quantum dot infrared photodetectors[20] and indeed in cascaded architectures as quantum dot quantum cascade detectors.[21,22]

Recently, there has been some interest in exploring interband transitions in self-assembled QDs with type-II band alignments, where both the QD material's valence and conduction band edges lie higher in energy than their respective counterparts in the surrounding matrix. One of the more promising of these material systems is In(Ga)Sb quantum dots in InAs matrices, which offer interband optical transitions in the MIR.[23–28] Early results with this QD material system showed promising Auger characteristics without deliberate band structure engineering,[29] with such QDs integrated into single stage, non-cascaded LEDs emitting 0.8 mW/cm^2 at 5 μm (78 K)[30] and 1.4 mW/cm^2 at 3.8 μm (300 K).[31] Of these two reports, only one contained light–current–voltage (LIV) data, showing that low parasitic shunt resistance substantially limited the potential wallplug and quantum efficiency of the devices. To the best of our knowledge, there have been no reports on cascaded MIR QD LEDs or QD LEDs demonstrating efficient electrical injection into the active region of the device.

Here, we present a cascaded mid-infrared LED leveraging InGaSb QD active regions to elucidate the effects of cascading on MIR QD LED performance. We demonstrate strongly reduced leakage current from the cascaded tunnel junction architecture, which has significant implications for small devices in MIR LED applications like thermal scene projection. Our devices are characterized electrically and optically, as a function of temperature. From the light–current–voltage data, we can extract the device efficiency and demonstrate that parasitic non-radiative recombination greatly limits the output power of the InGaSb QD LEDs. Finally, we suggest potential approaches to mitigate these parasitic channels in QD LEDs. The demonstrated architecture offers a path toward higher efficiency MIR LEDs or alternatively novel quantum sources in the mid-infrared.

II. DEVICE DESIGN, GROWTH, AND FABRICATION

High-quality tunnel junctions are key elements of interband, cascaded devices. The overall structure of such devices is that of several p–i–n active regions in series, p–i–$n\cdots p$–i–n, where the interior highly reverse-biased n–p junctions serve as tunnel junctions when the overall p–i–$n\cdots p$–i–n structure is under forward bias. Several design parameters can be optimized for high tunneling probability in the reverse-biased n–p tunnel junction, primarily doping and alloy composition. Increasing doping in the respective layers pushes the n layer toward lower energies and the p layer towards higher energies, which reduces the tunneling barrier even for homojunction designs. Type-II band offsets can also be used to increase the separation of the n region conduction band and p region valence band. However, tunnel junctions must be designed for the device in which they operate, which imposes restrictions on the specific choice of materials that can be used. Notably, tunnel junctions should provide sufficient carrier confinement in the active regions such that each carrier necessarily recombines once per stage, while providing minimal offset such that the flow of unexcited carriers out of the active region into the tunnel junction region is unimpeded.

InGaSb QDs have a type-II band offset with the surrounding InAs matrix, with electrons loosely bound in the conduction band of InAs and excited holes tightly bound in the InGaSb valence band (the inset to Fig. 1). Carrier transport throughout the i layer occurs solely in the InAs matrix, and consequently, the tunnel junctions must be designed to facilitate electron and hole injection into the InAs layer, rather than the InGaSb itself. InAs has the highest electron affinity of the so-called 6.1 Å materials (InAs, GaSb, AlSb, and related alloys), and, therefore, both its conduction and valence band edges lie low in energy. While electron barriers can be readily achieved using GaSb or AlSb, care must be taken to not create a barrier to hole injection from the tunnel junction p layer into the active region. This necessitates the choice of an alloy with the valence band edge (or, more accurately, hole quasi-Fermi

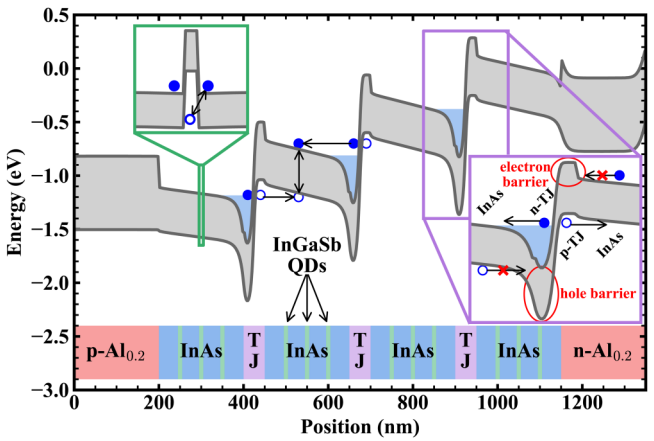

FIG. 1. Real space band diagram for the cascaded LED under 1.5 V forward bias. The solid black lines denote the band edges and shaded gray regions the bandgaps. The shaded blue regions are filled electron states due to degenerate doping in the n-type tunnel junction region. Electron (filled blue circle) and hole (open blue circle) pathways including generation at the highly reverse-biased tunnel junctions and recombination are denoted with arrows. The insets show expanded views of the type-II offset of the InGaSb QDs with respect to the InAs matrix (green border) and the features of tunnel junction designed band structure (purple border).

energy) near the valence band edge of InAs. Likewise, the conduction band edge (electron quasi-Fermi energy) of the *n* layer in the tunnel junction should sit at the InAs conduction band edge, while still providing as much valence band offset as possible to confine excited holes in the active region. There are relatively few alloys that meet the criteria for the *n* side of the tunnel junction. Here, we have employed $Al_{0.1}In_{0.9}As_{0.91}Sb_{0.09}$ as both the *n* and *p* layers in the tunnel junction. Undoped $Al_{0.1}In_{0.9}As_{0.91}Sb_{0.09}$ does not provide a hole barrier with respect to InAs; however, the use of moderately high *n* doping pushes the conduction and valence band edges to lower energy and thus *n*-$Al_{0.1}In_{0.9}As_{0.91}Sb_{0.09}$ can serve satisfactorily as the *n* layer of our tunnel junctions (at least at low temperatures). The band diagram of our four-stage LED is shown in Fig. 1, where the $Al_{0.1}In_{0.9}As_{0.91}Sb_{0.09}$ layers that form the tunnel junction are expected to form a 200 meV electron barrier and 400 meV hole barrier. An inset shows an expanded view schematic of the tunnel junction band structure and the mechanism by which it supplies carriers to the device active regions.

A four-stage device, comprising four active regions separated by three $Al_{0.1}In_{0.9}As_{0.91}Sb_{0.09}$ tunnel junctions and bookended by n- and p-$Al_{0.2}In_{0.8}As_{0.82}Sb_{0.18}$ contact regions, was subsequently grown, fabricated, and characterized. The sample was grown on an *n*-InAs substrate in an Veeco Gen-II molecular beam epitaxy machine with valved crackers supplying As and Sb dimers. Digital growth of the AlInAsSb layers was employed to alleviate immiscibility issues inherent in the conventional, random alloy. The $Al_{0.1}In_{0.9}As_{0.91}Sb_{0.09}$ and $Al_{0.2}In_{0.8}As_{0.82}Sb_{0.18}$ layers were doped to 1×10^{19} and 5×10^{17} cm^{-3}, respectively, for both *n*- and *p*-type layers. Doping was increased during the final 50 nm of the *p*-contact layer to reduce contact resistance. The 1.75 ml $In_{0.6}Ga_{0.4}Sb$ QDs were grown at 0.55 ml/s with a V/III beam-equivalent pressure ratio of 1.5, which was nominally just above stoichiometry. The sample was etched to the *n*-contact layer using a citric and phosphoric acid based wet-etch for mesa isolation, and a Pd/Ti/Pt/Au window contact was deposited on the top of the mesas. The mesa size was $560 \times 430\,\mu m^2$. The bottom electrical contact was made through the substrate, which was adhered with silver paste to a copper submount. Top contacts were wirebonded to ceramic standoffs, then the package was mounted in a liquid-nitrogen cooled cryostat with an uncoated ZnSe window for characterization.

III. RESULTS AND DISCUSSION

Emission spectra for the device were measured as a function of both input current and temperature by amplitude-modulation Fourier-transform infrared spectroscopy and are shown in Fig. 2. The spectra at cryogenic temperatures show several distinct peaks. The brightest, long-wavelength peak is associated with the type-II InGaSb QDs. There is also a shorter wavelength peak at 3 μm that likely corresponds to emission from the InAs matrix surrounding the dots and/or potentially from the AlInAsSb tunnel barrier layers. Combined, the presence of the short wavelength peak indicates both that the QD capture efficiency is less than unity and that some fraction of carriers recombine radiatively in InAs and/or AlInAsSb. At higher temperatures, the short wavelength peak diminishes below the noise floor, though it is ultimately unclear if

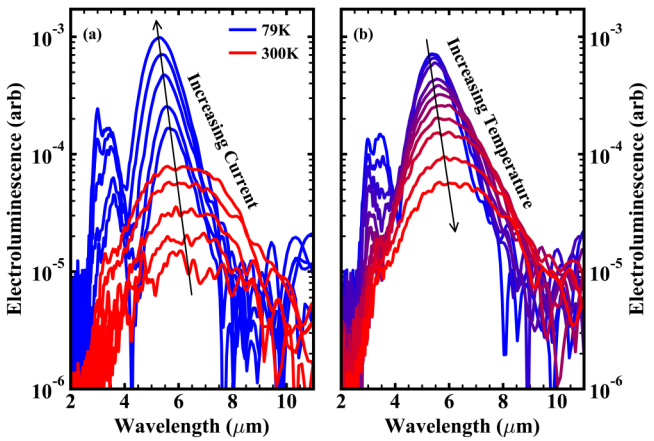

FIG. 2. (a) Current-dependent spectra at 79 K (blue) and 300 K (red) at currents of 37, 63, 119, 234, and 476 mA and (b) temperature-dependent emission spectra at a current injection of 234 mA.

the reduction in emission intensity indicates that the carriers no longer escape the QDs or, more likely, that emission from the InAs and AlInAsSb layers becomes so inefficient as to be undetectable.

Inhomogeneous broadening of QD electroluminescence occurs due to the nonuniform size distribution of an ensemble of self-assembled QDs. Consequently, the QD emission peak is quite broad at all temperatures, ranging from 51 (7.4 k_BT) to 122 meV (4.7 k_BT) between 79 and 300 K, far greater than the 1.8 k_BT expected for the emission linewidth of a bulk semiconductor. For laser applications, inhomogeneous broadening can cause problems due to reduced gain coefficient at a given wavelength. However, the potential applications for cascaded MIR LEDs in many cases do not require (or benefit from) narrow emission linewidth; MIR LEDs are often proposed for applications where they would replace inefficient, broadband, thermal sources. Many spectroscopic applications benefit from the spectrally wide emission of a blackbody source, and cascaded MIR LEDs have been designed with active regions emitting at slightly different wavelengths to mimic the spectral width of a blackbody source.[32] Thus, the class of device presented here may serve well in multi-species gas sensing applications that require broadband emission, while maintaining the advantages of LED illumination such as stability, power, and small size if the optical output power can be raised to be competitive with commercially available blackbody sources. It is further worth noting that in the case where these QDs still provide sufficient gain, they may serve as a broadband gain medium for external cavity and distributed feedback laser applications.

Current-density–voltage data were measured for the device as a function of temperature and are shown in Fig. 3. Leakage currents for this device are minimal, as evidenced by parallel resistances ranging from hundreds to thousands of ohms, as shown in the inset to Fig. 3(a). Equivalently, the current flow below the turn-on voltage is minimal. However, the turn-on voltage appears to vary with temperature in an unexpected fashion. Nominally, current in a cascaded LED with *N* stages emitting photons of average energy

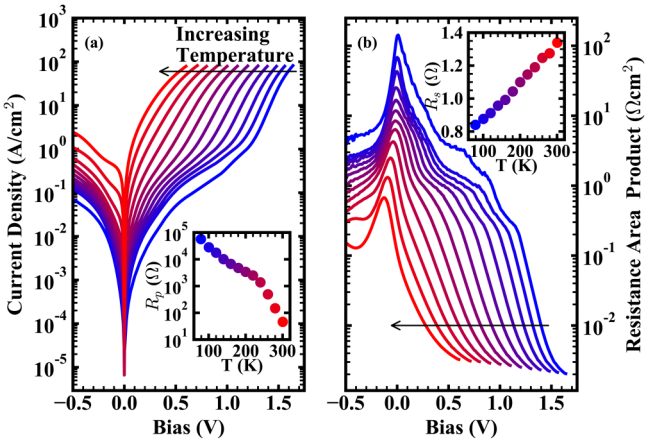

FIG. 3. Temperature-dependent (a) current-density–voltage and (b) dynamic resistance area product data for the device. The insets show the extracted parallel (a) and series resistance (b) of the diode as a function of temperature.

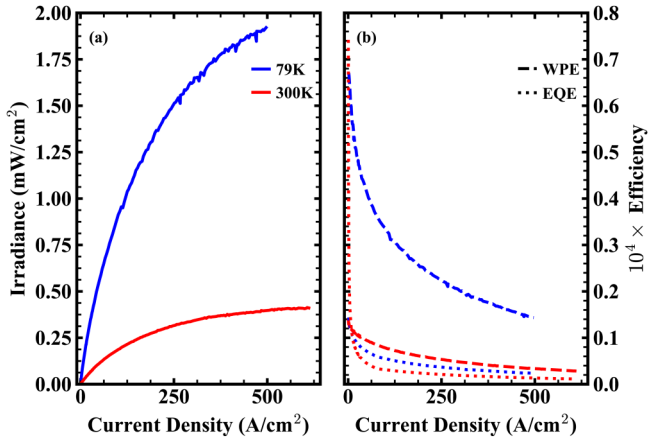

FIG. 4. (a) Light-current data at 79 K (blue) and 300 K (red). (b) Wallplug efficiency (dashed) and external quantum efficiency (dotted) at 79 K (blue) and 300 K (red).

E_{ph} should begin to flow at a voltage of NE_{ph}/e for e the elementary charge, though the turn-on voltage is typically a bit higher due to voltage drop across the tunnel junctions. In this device at 79 K, the turn-on voltage and average photon energy are approximately 1.35 V and 280 meV, respectively, indicating very little parasitic voltage is being dropped across the tunnel junctions. The average photon energy of the temperature-dependent spectra shown in Fig. 2(b) decreases approximately 20% between 79 and 300 K and thus a 20% decrease in the turn-on voltage can be explained by the temperature dependence of the bandgap. However, the turn-on voltage (here defined as the bias at which the current density is 10 A/cm^2) decreases from 1.35 V to 180 mV. This drastic reduction in operating voltage suggests that, while the n and p layers in the tunnel junctions provide sufficient carrier confinement in the active region at low temperatures, the added thermal energy in the carriers at higher temperatures allows them to thermionically emit over the barriers. Thermionic emission then acts as a parallel current path that reduces the device effectively to a single-stage device at room temperature.

Figure 4 shows the light-current-density and efficiency curves at 79 and 300 K. Light power measurements were made with a calibrated mercury cadmium telluride detector in a 1:1 imaging setup. The maximum output power of 4.7 μW at 79 K corresponds to a peak irradiance of 1.9 mW/cm^2, more than double our previous 79 K result for a single-stage device. In principle, an N stage device should emit N more photons than a single-stage device; however, this scaling is generally underperformed due to thermally induced rollover under high-injection. In practice, an $N/2$ increase in the maximum output irradiance is fairly typical of cascaded MIR LEDs.[33] At 300 K, the device emits up to 0.4 mW/cm^2 before thermally induced rollover, despite the effective conversion from 4-stage device to 1-stage. The minimal factor of ~5 reduction in peak output irradiance is a hallmark of the low Auger coefficient in the InGaSb QDs. Auger recombination scales exponentially with temperature and thus a small Auger coefficient is important for high operating temperature devices. Attempts to model the quantum efficiency of our device to extract the Shockley–Read–Hall, radiative, and Auger rates did not yield satisfactory fits to the data. It is unclear if it is solely carrier degeneracy effects in the QDs that prevents the application of power-law dependences for the recombination processes[34] or a more complicated process related to carrier capture by each stage of the device and ultimately the QDs themselves which drives the disagreement between the model and experiment.

The low series and high parallel resistances (insets to Fig. 3), in conjunction with the expected 1.35 V turn-on voltage at 79 K indicate that our cascaded device has performed as expected at low temperatures. Despite the low Ohmic losses, the wallplug and external quantum efficiencies (WPE and EQE, respectively) shown in Fig. 4(b) trail the state-of-the-art demonstrated in more mature quantum well and superlattice systems.[35] It is further worth noting that the EQE curves are monotonically decreasing with increasing current density, which is commonly attributed to either Auger recombination or carrier leakage. However, the Auger coefficient has been measured to be on the order of 10^{-28} cm^6/s in InGaSb QDs, using power dependent photoluminescence measurements.[29] We, therefore, suspect that the low quantum efficiency is a consequence of inefficient electron capture in the QDs. Achieving higher QD density may provide one path toward a higher total electron capture rate. Additionally, the capture rate for an individual QD is likely low because the type-II alignment does not confine electrons near the QD, and the low effective mass and high mobility of the InAs matrix, which provide an efficient pathway for electrons to escape the QD. As a result of the low total electron capture rate, the efficiency and output characteristics of the cascaded device, even at 79 K, remain limited. We suspect that future work integrating InGaSb quantum dots into dot-in-well (DWELL) type structures may increase the electron capture and concomitantly the

quantum efficiency by providing quantum confinement for electrons around the QD layers.

IV. CONCLUSION

We have presented a cascaded quantum dot emitter operating in the MIR. The current–voltage characteristics of the LED at cryogenic temperatures show that the tunnel junctions perform well with low parasitic voltage drop and series resistance. At higher temperatures, the turn-on voltage of the devices anomalously decreased, indicating that thermal excitation over the tunnel junction barriers effectively transforms the cascaded device into a single-stage structure. Due to the low Auger coefficient in InGaSb QDs, the maximum output irradiance only decreased a factor of 5 between 79 and 300 K. These results demonstrate that a cascaded heterostructure can be achieved with InGaSb QD active regions and that further improvements to the QD capture and radiative efficiencies may provide a path toward high-efficiency MIR emitters with the potential to serve MIR quantum applications.

ACKNOWLEDGMENTS

This material was based upon work supported by the United States Air Force under STTR Contract No. FA8650-19-C-1949. Any opinions, findings, and conclusions or recommendations expressed in this material are those of the author(s) and do not necessarily reflect the views of the U.S. Air Force. The authors gratefully acknowledge support from the National Science Foundation (No. ECCS-1926187). This work was partly done at the Texas Nanofabrication Facility supported by NSF Grant No. NNCI-1542159.

AUTHOR DECLARATIONS

Conflict of Interest

The authors have no conflicts to disclose.

DATA AVAILABILITY

The data that support the findings of this study are available from the corresponding author upon reasonable request.

REFERENCES

[1]A. Krier, V. V. Sherstnev, and H. H. Gao, "A novel LED module for the detection of H_2S at 3.8 μm," J. Phys. D: Appl. Phys. **33**, 1656 (2000).
[2]D. Jung, S. Bank, M. L. Lee, and D. Wasserman, "Next-generation mid-infrared sources," J. Opt. **19**, 123001 (2017).
[3]H. H. Tseng, K. Y. Wu, H. Li, V. Mashanov, H. H. Cheng, G. Sun, and R. A. Soref, "Mid-infrared electroluminescence from a Ge/$Ge_{0.922}Sn_{0.078}$/Ge double heterostructure p-i-n diode on a Si substrate," Appl. Phys. Lett. **102**, 182106 (2013).
[4]X. Zhang, J.-X. Shen, and C. G. Van De Walle, "Anomalous Auger recombination in PbSe," Phys. Rev. Lett. **125**, 037401 (2020).
[5]B. B. Haidet, L. Nordin, A. J. Muhowski, K. D. Vallejo, E. T. Hughes, J. Meyer, P. J. Simmonds, D. Wasserman, and K. Mukherjee, "Interface structure and luminescence properties of epitaxial PbSe films on InAs(111)A," J. Vac. Sci. Technol. A **39**, 023404 (2021).
[6]C. H. Grein, P. M. Young, and H. Ehrenreich, "Minority carrier lifetimes in ideal InGaSb/InAs superlattices," Appl. Phys. Lett. **61**, 2905 (1992).
[7]M. E. Flatté, C. H. Grein, H. Ehrenreich, R. H. Miles, and H. Cruz, "Theoretical performance limits of 2.1–4.1 μm InAs/InGaSb, HgCdTe, and InGaAsSb lasers," J. Appl. Phys. **78**, 4552 (1995).
[8]E. R. Youngdale, J. R. Meyer, C. A. Hoffman, F. J. Bartoli, C. H. Grein, P. M. Young, H. Ehrenreich, R. H. Miles, and D. H. Chow, "Auger lifetime enhancement in InAs–$Ga_{1-x}In_xSb$ superlattices," Appl. Phys. Lett. **64**, 3160 (1994).
[9]J. Faist, F. Capasso, D. L. Sivco, C. Sirtori, A. L. Hutchinson, and A. Y. Cho, "Quantum cascade laser," Science **264**, 553–556 (1994).
[10]J. R. Meyer, I. Vurgaftman, R. Q. Yang, and L. R. Ram-Mohan, "Type-II and type-I interband cascade lasers," Electron. Lett. **32**, 45–46 (1996).
[11]J. Abell, C. S. Kim, W. W. Bewley, C. D. Merritt, C. L. Canedy, I. Vurgaftman, J. R. Meyer, and M. Kim, "Mid-infrared interband cascade light emitting devices with milliwatt output powers at room temperature," Appl. Phys. Lett. **104**, 261103 (2014).
[12]M. Ermolaev, Y. Lin, L. Shterengas, T. Hosoda, G. Kipshidze, S. Suchalkin, and G. Belenky, "GaSb-based type-I quantum well 3–3.5 μm cascade light emitting diodes," IEEE Photonics Technol. Lett. **30**, 869–872 (2018).
[13]E. J. Koerperick, J. T. Olesberg, T. F. Boggess, J. L. Hicks, L. S. Wassink, L. M. Murray, and J. P. Prineas, "InAs/GaSb cascaded active region superlattice light emitting diodes for operation at 3.8 μm," Appl. Phys. Lett. **92**, 121106 (2008).
[14]E. J. Koerperick, D. T. Norton, J. T. Olesberg, B. V. Olson, J. P. Prineas, and T. F. Boggess, "Cascaded superlattice InAs/GaSb light-emitting diodes for operation in the long-wave infrared," IEEE J. Quantum Electron. **47**, 50–54 (2011).
[15]A. Y. Liu, C. Zhang, J. Norman, A. Snyder, D. Lubyshev, J. M. Fastenau, A. W. Liu, A. C. Gossard, and J. E. Bowers, "High performance continuous wave 1.3 μm quantum dot lasers on silicon," Appl. Phys. Lett. **104**, 041104 (2014).
[16]S. Chen, W. Li, J. Wu, Q. Jiang, M. Tang, S. Shutts, S. N. Elliott, A. Sobiesierski, A. J. Seeds, I. Ross, P. M. Smowton, and H. Liu, "Electrically pumped continuous-wave III-V quantum dot lasers on silicon," Nat. Photonics **10**, 307–311 (2016).
[17]S. Franchi, G. Trevisi, L. Seravalli, and P. Frigeri, "Quantum dot nanostructures and molecular beam epitaxy," Prog. Cryst. Growth Charact. Mater. **47**, 166–195 (2003).
[18]D. Wasserman and S. A. Lyon, "Midinfrared luminescence from InAs quantum dots in unipolar devices," Appl. Phys. Lett. **81**, 2848–2850 (2002).
[19]K. W. Berryman, S. A. Lyon, and M. Segev, "Mid-infrared photoconductivity in InAs quantum dots," Appl. Phys. Lett. **70**, 1861–1863 (1997).
[20]D. Pan, E. Towe, and S. Kennerly, "A five-period normal-incidence (In, Ga) As/GaAs quantum-dot infrared photodetector," Appl. Phys. Lett. **75**, 2719–2721 (1999).
[21]A. V. Barve and S. Krishna, "Photovoltaic quantum dot quantum cascade infrared photodetector," Appl. Phys. Lett. **100**, 021105 (2012).
[22]Z. Shen, Z. Deng, X. Zhao, J. Huang, C. Cao, X. Zou, F. Liu, Q. Gong, and B. Chen, "Submonolayer quantum dot quantum cascade long-wave infrared photodetector grown on Ge substrate," Appl. Phys. Lett. **118**, 081102 (2021).
[23]S. V. Ivanov, A. N. Semenov, V. A. Solov'ev, O. G. Lyublinskaya, Y. V. Terent'ev, B. Y. Meltser, L. G. Prokopova, A. A. Sitnikova, A. A. Usikova, A. A. Toropov, and P. S. Kop'ev, "Molecular beam epitaxy of type II InSb/InAs nanostructures with InSb sub-monolayers," J. Cryst. Growth **278**, 72–77 (2005).
[24]K. D. Moiseev, Y. A. Parkhomenko, A. V. Ankudinov, E. V. Gushchina, M. P. Mikha, A. N. Titkov, and Y. P. Yakovlev, "InSb/InAs quantum dots grown by liquid phase epitaxy," Tech. Phys. Lett. **33**, 295–298 (2007).
[25]S. Shusterman, Y. Paltiel, A. Sher, V. Ezersky, and Y. Rosenwaks, "High-density nanometer-scale InSb dots formation using droplets heteroepitaxial growth by MOVPE," J. Cryst. Growth **291**, 363–369 (2006).
[26]Q. Zhuang, P. J. Carrington, and A. Krier, "Growth optimization of self-organized InSb/InAs quantum dots," J. Phys. D: Appl. Phys. **41**, 232003 (2008).
[27]F. Hatami, S. M. Kim, H. B. Yuen, J. S. Harris, F. Hatami, S. M. Kim, H. B. Yuen, and J. S. Harris, "InSb and InSb:N multiple quantum dots," Appl. Phys. Lett. **89**, 133115 (2006).

[28]R. Liu, Y. Zhong, L. Yu, H. Kim, S. Law, J.-M. Zuo, and D. Wasserman, "Mid-infrared emission from In(Ga)Sb layers on InAs(Sb)," Opt. Express **22**, 24466 (2014).
[29]T. Zabel, C. Reuterskiöld Hedlund, O. Gustafsson, A. Karim, J. Berggren, Q. Wang, C. Ernerheim-Jokumsen, M. Soldemo, J. Weissenrieder, M. Götelid, and M. Hammar, "Auger recombination in In(Ga)Sb/InAs quantum dots," Appl. Phys. Lett. **106**, 013103 (2015).
[30]A. F. Briggs, L. J. Nordin, A. J. Muhowski, P. Petluru, D. Silva, D. Wasserman, and S. R. Bank, "Mid-infrared electroluminescence from type-II In(Ga)Sb quantum dots," Appl. Phys. Lett. **116**, 061103 (2020).
[31]P. J. Carrington, V. A. Solov'ev, Q. Zhuang, A. Krier, and S. V. Ivanov, "Room temperature midinfrared electroluminescence from InSb/InAs quantum dot light emitting diodes," Appl. Phys. Lett. **93**, 091101 (2008).
[32]R. J. Ricker, S. R. Provence, D. T. Norton, T. F. Boggess, and J. P. Prineas, "Broadband mid-infrared superlattice light-emitting diodes," J. Appl. Phys. **121**, 185701 (2017).
[33]E. J. Koerperick, J. T. Olesberg, J. L. Hicks, J. P. Prineas, and T. F. Boggess, "Active region cascading for improved performance in InAs–GaSb superlattice LEDs," IEEE J. Quantum Electron. **44**, 1242–1247 (2008).
[34]P. Blood, H. Pask, H. D. Summers, and I. Sandall, "Localized Auger recombination in quantum-dot lasers," IEEE J. Quantum Electron. **43**, 1140–1146 (2007).
[35]D. A. Montealegre, K. N. Schrock, A. C. Walhof, A. M. Muellerleile, and J. P. Prineas, "High-power mid-wave infrared LED using W-superlattices and textured surfaces," Appl. Phys. Lett. **118**, 071105 (2021).